Author Manuscript

Author Manuscript

Author Manuscript

Author Manuscript

HHS Public Access

Author manuscript

*ACS Appl Mater Interfaces*. Author manuscript; available in PMC 2019 March 28.

Published in final edited form as:

*ACS Appl Mater Interfaces*. 2018 January 24; 10(3): 2377–2390. doi:10.1021/acsami.7b18458.

# Immunomodulatory ECM-like Microspheres for Accelerated Bone Regeneration in Diabetes Mellitus

**Zhiai Hu**[†,§], **Chi Ma**[§], **Xin Rong**[‡], **Shujuan Zou**[*,†], and **Xiaohua Liu**[*,§]

[†] State Key Laboratory of Oral Diseases, National Clinical Research Center for Oral Disease, West China Hospital of Stomatology, Sichuan University, Chengdu 610041, China

[‡] Department of Orthopedics, West China Hospital, Sichuan University, Chengdu 610041, China

[§] Department of Biomedical Sciences, Texas A&M University College of Dentistry, Dallas, Texas 75246, United States

## Abstract

Bone repair and regeneration process is markedly impaired in diabetes mellitus (DM) that affects hundreds of millions of people worldwide. As a chronic inflammatory disease, DM creates a proinflammatory microenvironment in defective sites. Most of the studies on DM-associated bone regeneration, however, neglect the importance of immunomodulation under the DM condition and adopt the same approaches to normal bone healing, leading to limited bone healing. In this study, we developed a unique bioinspired injectable microsphere as an osteoimmunomodulatory biomaterial that modulates macrophages to create a prohealing microenvironment under the DM condition. The microsphere was self-assembled with heparin-modified gelatin nanofibers, and interleukin 4 (IL4) was incorporated into the nanofibrous heparin-modified gelatin microsphere (NHG-MS). IL4 has binding domains with heparin, and the binding of IL4 to heparin stabilizes this cytokine, protects it from denaturation and degradation, and subsequently prolongs its sustained release to modulate macrophage polarization. The IL4-loaded NHG-MS switched the proinflammatory M1 macrophage into a prohealing M2 phenotype, recovered the M2/M1 ratio to a normal level, efficiently resolved the inflammation, and ultimately enhanced osteoblastic differentiation and bone regeneration. The development of osteoimmunomodulatory biomaterials that harness the power of macrophages for immunomodulation, therefore, is a novel and promising strategy to enhance bone regeneration under DM condition.

## Graphical Abstract:

[*]**Corresponding Authors** drzsj@scu.edu.cn (S.Z.)., xliu@tamhsc.edu (X.L.).

Author Contributions

The manuscript was written through contributions of all authors. All authors have given approval to the final version of the manuscript.

Notes

The authors declare no competing financial interest.

Supporting Information

The Supporting Information is available free of charge on the ACS Publications website at DOI: 10.1021/acsami.7b18458.

FTIR spectra; degradation of nanofibrous heparin-modified gelatin microsphere (NHG-MS) controlled by the cross-linking density (PDF)

Author Manuscript Author Manuscript Author Manuscript Author Manuscript

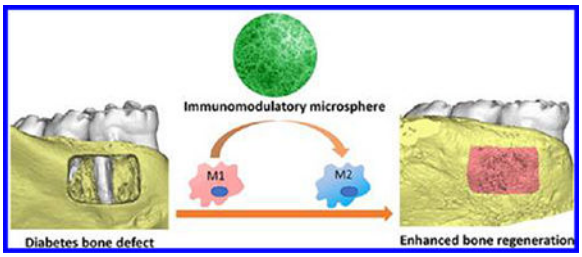


**Keywords**

immunomodulatory; macrophage; microspheres; nanofibrous; bone tissue engineering; diabetes mellitus

## 1. INTRODUCTION

Diabetes mellitus (DM) is one of the most common diseases affecting more than 380 million people worldwide in 2013, and the number of DM patients is estimated to further increase to over 590 million by 2035.[1–3] As a chronic systemic disease with vascular complications, DM contributes to osteoporosis, increased risk of fracture, delayed bone-healing rates, and compromised bone repair quality.[4–10] In fact, it was reported that DM patients had a 1.6-fold delay in fracture healing and the risk of a 2.75-fold increase in implant failure.[11,12] Consequently, the process of bone repair and regeneration under diabetic condition is markedly impaired. With the rapidly expanding DM population requiring a higher rate of bone repair/regeneration, there is an intense demand to develop effective methods to accelerate bone regeneration for patients with DM.

Currently, most of the approaches to DM-associated bone regeneration focus on either enhancing the osteogenic differentiation of bone-forming cells (osteoblasts) or decreasing the number and activity of bone resorption cells (osteoclasts).[13–17] For example, bone morphogenetic protein 2 (BMP2) was embedded in a collagen sponge to stimulate osteoblast differentiation and bone healing in the calvarial defect of a DM mouse model.[13] Although BMP2 may be beneficial for treating deficient bone formation under diabetic condition, it is expensive and has well-documented side effects, including postoperative inflammation, ectopic bone formation, osteoclast-mediated bone resorption, and inappropriate adipogenesis.[18] More importantly, DM is a chronic inflammatory disease, and bone regeneration is a dynamic complex process, in which immune cells play critical roles in controlling inflammation and maintaining tissue homeostasis. However, the growth factor (or hormone) delivery approach was directly targeted at bone cells (osteoblasts and osteoclasts) and the importance of immunomodulation under diabetic condition was neglected.

Macrophages are important immune cells that play a central role in inflammation activation and resolution.[19,20] Macrophages are mainly divided into two phenotypes: classically activated proinflammatory M1 macrophages and alternatively activated prohealing M2 macrophages. Characterized by strong plasticity, macrophages are able to dynamically switch from one phenotype to the other depending on the surrounding microenvironment.

Author Manuscript Author Manuscript Author Manuscript Author Manuscript

The dynamic shift from M1 to M2 macrophages is of great importance in tissue healing.[21] Type 2 DM (T2DM), which accounts for 90–95% of the total number of diagnosed cases of DM, has been considered an inflammatory disease as evidenced by the elevated levels of proinflammatory cytokines, such as interleukin-1$\beta$ (IL-1$\beta$), interleukin 6 (IL6), and C-reactive protein.[22,23] Therefore, the development of osteoimmunomodulatory biomaterials that harness the power of macrophages for immunomodulation would be a novel and promising strategy to enhance bone regeneration for DM patients.

In this study, we developed a unique bioinspired injectable microsphere as an osteoimmunomodulatory scaffolding biomaterial (Scheme 1). The microsphere was self-assembled with heparin-modified gelatin nanofibers that mimic the architecture of natural bone extracellular matrices (ECMs) and provide an osteoconductive microenvironment for bone marrow stem cells.[24–26] As a scaffolding biomaterial, the injectable microsphere has the advantages of being administrated in a minimally invasive manner and easily adapted to complex defects.[27] Furthermore, interleukin 4 (IL4), which is the main cytokine responsible for the polarization of proinflammatory M1 into an anti-inflammatory M2 phenotype, was incorporated into the nanofibrous heparin-modified gelatin microsphere (NHG-MS). IL4 has binding domains with heparin,[28] and the binding of IL4 to heparin stabilizes this cytokine, protects it from denaturation and degradation, and subsequently prolongs its sustained release to modulate macrophage polarization. We hypothesized that this osteoimmunomodulatory microsphere would transform macrophages to an anti-inflammatory M2 phenotype and create a proregenerative microenvironment for enhanced bone regeneration under DM condition.

## 2. MATERIALS AND METHODS

### 2.1. Materials.

Gelatin (type B, from bovine skin, 225 g Bloom), heparin (sodium salt from porcine intestinal mucosa, MW ≈ 17–19 kDa), bovine serum albumin (BSA), fluorescein isothiocyanate (FITC), and type I collagenase from *Clostridium histolyticum* were purchased from Sigma-Aldrich (St Louis, MO). 1-Ethyl-3-(3-dimethylaminopropyl)carbodiimide hydrochloride (EDC) was purchased from Thermo Scientific (Rockford, IL). Morpholinoethanesulfonic acid (MES) and *N*-hydroxysuccinimide (NHS) were purchased from Acros Organics (New Jersey). Dialysis membrane (molecular weight cutoff (MW cutoff 50 kDa)) was purchased from Spectrum Laboratories (Dallas, TX). Mineral oil, isopropanol, 1,4-dioxane, ethanol, and glycine were purchased from VWR.

### 2.2. Synthesis and Characterization of Heparin-Modified Gelatin.

Heparin-modified gelatin (HG) was synthesized as previously reported with minor modifications.[29] First, 4 g of gelatin and 1 g of heparin were dissolved separately in 100 mL of aqueous solution containing 50 mM MES and 0.2 M NaCl. Next, 0.12 g of EDC and 0.26 g of NHS were added to the heparin solution under stirring for 15 min, followed by addition of 100 mL of gelatin solution and reaction at room temperature for 12 h. The final product was dialyzed for 3 days in 0.2 M NaCl solution before being transferred into deionized

Author Manuscript Author Manuscript Author Manuscript Author Manuscript

water. The HG was characterized by Fourier transform infrared (FTIR) spectroscopy. The heparin content was measured using a toluidine blue assay, and the in vitro degradation of the HG was performed as previously reported.[29]

### 2.3. Fabrication of NHG-MS and Solid Gelatin Microspheres (SG-MS).

NHG-MS was fabricated by combining the water/oil (W/O) emulsification technique and the thermally induced phase separation process. First, HG was dissolved in ethanol/water (50/50, v/v) solvent mixture at 50 °C. Under rigorous mechanical stirring (750 rpm), 7 mL of HG solution was gradually added into mineral oil to form a water-in-oil (W/O) emulsion. Next, the mixture was immediately poured into 800 mL of isopropanol/1,4-dioxane/ethanol (4/3/1,v/v/v,–20 °C) mixture under gentle stirring to induce phase separation and solvent exchange. The microspheres obtained were cross-linked with EDC and NHS in MES buffer (pH 5.3, 0.05 M) at 4 °C for 48 h as previously reported.[30] To maintain the nanofibrous architecture of the microsphere in water, acetone/water solvent mixture with a ratio of 9/1 (v/v) was chosen for the cross-linking reaction. NHG-MS was incubated in a 0.5 M glycine solution for 3 h to neutralize the unreacted cross-linking agent, washed with distilled water three times, and sieved to obtain different size. Finally, the NHG-MS was lyophilized and stored in a desiccator for later use. The in vitro enzymatic degradation assay of NHG-MS was performed as previously reported.[29]

SG-MS was prepared using a conventional solvent evaporation technique. First, gelatin was dissolved in aqueous solution at 50 °C with a concentration of 20% (w/v). Next, the gelatin solution was gradually added to olive oil and the mixture was stirred (450 rpm) for 24 h. The solid microspheres were collected for chemical cross-linking using the same system as the NHG-MS. After neutralizing the unreacted cross-linking agent with 0.5 M glycine solution, the SG-MS was washed with distilled water three times and lyophilized before being stored in a desiccator for later use.

### 2.4. Incorporation of IL4 into NHG-MS and Release Assay.

Recombinant rat IL4 (R&D system) was reconstituted at a concentration of 4 $\mu$g/mL in sterile Dulbecco's phosphate-buffered saline (DPBS) (Gibco) containing 0.1% bovine serum albumin (BSA, Sigma-Aldrich). IL4 solution (500 $\mu$L) was loaded into 10 mg of NHG-MS at 4 °C for 18 h. Next, the NHG-MS was soaked in 10 mL of DPBS containing 0.1% BSA (w/v) incubated at 37 °C for 1 h and collected by centrifugation. The supernatant was aspirated and defined as "unloaded" IL4, and the loaded IL4 was determined by subtracting the unloaded IL4 from the initial total IL4.

Immunofluorescence staining was performed to visualize the distribution of IL4 on the NHG-MS. First, the IL4-loaded NHG-MS was immersed in DPBS supplemented with 20% goat serum and 3% BSA at room temperature for 1 h to block the nonspecific adsorption. Next, the blocking solution was aspirated and the NHG-MS was incubated in antirat IL4 primary antibody solution (1:100 in 2% goat serum, Peprotech) at room temperature for 2 h. After washing with PBST (0.05% Tween-20 in PBS) three times, the NHG-MS was incubated in Alexa Fluor 647 (red) antirabbit IgG solution (1:200 in 2% goat serum, Abcam)

Author Manuscript Author Manuscript Author Manuscript Author Manuscript

at room temperature for 1 h. The samples were observed under a confocal laser scan microscope (TCS SP5, Leica, Buffalo).

To determine the IL4 release profile, the IL4-loaded NHG-MS was immersed in 1 mL of RPMI-1640 (Gibco) medium containing 0.1% BSA (w/v) at 37 °C. At designated time points (1, 3, 7, 14, and 21 days), the supernatant (1 mL) was collected and the same amount of fresh medium was replaced in the sample. For the last collection, 1 mL of type I collagenase (30 units/mL, Sigma-Aldrich) was added to degrade the NHG-MS and the IL4 in the supernatant was defined as unreleased IL4 in the NHG-MS. All of the samples were analyzed by enzyme-linked immunosorbent assay (ELISA) (Rat IL4 Quantikine ELISA Kit, R&D system). Three samples were performed in each time point, and the experiment was repeated twice.

### 2.5. In Vitro Bioactivity Assay of the Released IL4 from NHG-MS.

To test the bioactivity of IL4 released from NHG-MS, the IL4-containing supernatant collected at day 1 and day14 was diluted to 20 ng/mL for macrophage polarization and inflammatory cytokine assay. The bone marrow-derived macrophages (BMDMs) were isolated from the femurs and tibias of Sprague-Dawley (SD) rats as described.[31] The BMDMs were cultured in RPMI-1640 supplemented with 10% fetal bovine serum (Gibco, Carlsbad, CA), 2 mM glutamine, 1% penicillin-streptomycin (Sigma-Aldrich), and 20 ng/mL recombinant rat macrophage colony-stimulating factor (M-CSF, Peprotech) for 7 days. The BMDMs were seeded on four-well chamber slides at $1 \times 10^4$ cells/well and stimulated with 10 ng/mL lipopolysaccharide (LPS, Sigma-Aldrich) and 10 ng/mL interferon (IFN)-$\gamma$ (Peprotech) for 24 h to induce M1 polarization. The medium was then replaced with fresh medium supplemented with 10 ng/mL LPS, 10 ng/mL IFN-$\gamma$, and 20 ng/mL soluble IL4, the IL4 released from the NHG-MS at 1 day or 14 days, or blank vehicle as a negative control. After cultivation for 24 h, all of the supernatants were collected to quantify the production of tumor necrosis factor (TNF)-$\alpha$ and IL6 using ELISA (R&D system). Immunofluorescence staining was performed to identify M2 macrophages. The cells were double-stained with primary antibodies of mouse monoclonal anti-CD68 (1:200, ab955, Abcam) and rabbit polyclonal anti-CD206 (1:1000, ab64693, Abcam). Then, the samples were incubated with Alexa Fluor 488 (green) antirabbit IgG and Alexa Fluor 647 (red) antimouse IgG secondary antibody (1:200, Abcam). Nuclei were counterstained with Hoechst (Invitrogen). Images were acquired using a confocal laser scan microscope. For semiquantitative analysis, the ratio $CD68^+CD206^+$ cells/$CD68^+$ cells was calculated.

### 2.6. Establishment of DM Rat Model.

All animal protocols were approved by the University Committee on Use and Care of Animals of Texas A&M University College of Dentistry. Six-week-old male Sprague-Dawley (SD) rats (Charles River Laboratories) were used in this study. Type 2 diabetes was induced according to the method of Reed et al.[32] The rats were fed with a high-fat diet (60 kcal % fat, Charles River, D12492) for 4 weeks, followed by a low-dose streptozotocin (30 mg/kg, Sigma-Aldrich) injection to induce experimental type 2 diabetes. Fasting glucose over 11.1 mmol/L stable for 2 weeks was considered diabetes. After diabetic confirmation, all animals were fed regular diets.

Author Manuscript Author Manuscript Author Manuscript Author Manuscript

### 2.7. In Vivo Study.

A total of 36 SD rats were randomly assigned to four groups: normal control ($n$ = 9), DM control ($n$ = 9), DM with NHG-MS scaffold ($n$ = 9), and DM with IL4-loaded NHG-MS ($n$ = 9). A rat mandibular periodontal fenestration defect model was created as previously reported with modifications.[33] All possible efforts were made to minimize pain and discomfort of the rats during the surgery. The rats were anesthetized with 4% (w/v) isoflurane, followed by an intraperitoneal injection of ketamine (60 mg/kg) and xylazine (12 mg/kg), combined with a subcutaneous injection of buprenorphine for analgesia. The furs surrounding the surgical area was removed, and the skin was disinfected. The entire surgery was performed under a magnifying stereoscope (10×) for proper identification of anatomical landmarks and site preparation. A 1.5 cm incision was performed along the inferior border of the mandible to expose the masseter muscle. The area of interest was dissected through the masseter muscle slightly under the lower ligamentous line by a second incision until the body of the mandible was reached (buccal plate). After locating the buccal plate, a No. 4 round bur was used to initiate access to the buccal root, followed by a No. 1/2 bur to complete the osteotomy to create a standard defect size of 3 mm × 2 mm × 1 mm. The sterilized NHG-MS with or without IL4 was carefully loaded into the defect area. To avoid NHG-MS potentially moving out of the defect area, the masseter muscle over the surgical site was repositioned using absorbable sutures, followed by suturing the skin incision. After surgery, all of the rats received subcutaneous injections of buprenorphine (0.1 mg/kg) for analgesia twice per day for 3 days and were fed a soft-food diet for 7 days. The rats were sacrificed 7, 14, and 28 days after surgery. The samples were harvested for histology, immunohistochemistry, immunofluorescence, and $\mu$-CT assay.

### 2.8. $\mu$CT, Histology, Immunohistochemistry, and Immunofluorescence Analyses.

$\mu$CT scans of the rat mandibles were completed at 10 $\mu$m resolution using a $\mu$-CT35 imaging system (Scanco Medical). Samples were reconstructed and segmented using the Mimics software 10.01 (Materialise, Belgium). The bone volume (BV) to total volume (TV) ratio of the defect site was analyzed using Scanco Medical software.

The rat mandibles were fixed in 4% paraformaldehyde at 4 °C for 48 h. The tissues were washed in PBS for 1 h and demineralized in 15% ethylenediaminetetraacetic acid for 6 weeks at room temperature. After decalcification was completed, the specimens were dehydrated using an ascending ethanol series and then embedded in paraffin. Consecutive horizontal sections (4 $\mu$m) obtained from the middle third of the mandibular defect were used for histology, immunofluorescence, and immunochemistry analyses. Hematoxylin & eosin (H&E) staining was performed for histologic observation. Alkaline phosphatase (ALP) staining was performed to examine osteogenic activity according to Wang et al.[34]

Immunofluorescence staining was performed as previously reported.[35] The sections were double-stained with primary antibodies of anti-CD68 and anti-iNOS (1:200, ab15323, Abcam) or anti-CD68 and anti-CD206 to detect M1 or M2 macrophages, respectively. The images were obtained with a confocal laser scanning microscope. For semiquantitative analysis, the number of $CD68^+$ cells/$mm^2$ and the ratios of $iNOS^+CD68^+$ cells/$CD68^+$ cells,

Author Manuscript Author Manuscript Author Manuscript Author Manuscript

$CD206^+CD68^+$ cells/$CD68^+$ cells, and M2/M1 macrophages in the defect area were calculated by Image-Pro Plus 6.0 (Media Cybernetics).

Immunohistochemical analysis was performed with a Vectastain Elite ABC-HRP Kit (Vector Laboratories, Burlingame, CA) according to the manufacturer's instructions. Antibodies used included rabbit polyclonal anti-TNF-$\alpha$ (1:200, ab6671, Abcam), rabbit polyclonal anti-Runt-related transcription factor 2 (Runx2, 1:1000, ab23981, Abcam), and anti-Osterix (1:400, ab22552, Abcam). Histomorphometric analyses were performed with Image-Pro plus 6.0 software. At least four slides from each sample were used for quantification. The defect area was defined as the region of interest (ROI). For TNF-$\alpha$ staining, the area of TNF-$\alpha^+$ located in the ROI was calculated and expressed as a percentage of TNF-$\alpha^+$ area in the ROI (TNF-$\alpha^+$ area/ROI). A similar method was used to quantify ALP staining. For Osterix or Runx2 immunochemistry, the number of $Osterix^+$ or $Runx2^+$ cells located in the ROI was calculated and expressed as the number of $Osterix^+$ cells/$mm^2$ or $Runx2^+$ cells/$mm^2$. The mean integrated optical density (IOD) was also measured.

### 2.9. Statistical Analysis.

Data were analyzed with SPSS software (version 16.0; SPSS, Chicago, IL). All results were expressed as mean ± standard deviation. The difference between four groups was compared by one-way ANOVA. The difference between two groups was compared by Student's *t* test. The significance level was set at $P < 0.05$.

## 3. RESULTS

### 3.1. Synthesis and Characterization of Nanofibrous Heparin-Conjugated Gelatin Microspheres.

To provide binding domains for IL4 and to control its release, heparin was incorporated onto gelatin chains via an EDC/NHS coupling reaction, which was confirmed using an FTIR spectrometer (Supporting Information, Figure S1). The amount of heparin immobilized in the gelatin was modulated by the heparin concentration and cross-linking time.[29] On the basis of experimental conditions of 5 mg/mL of heparin in the reaction solution and cross-linking time of 12 h, the amount of heparin in the heparin-conjugated gelatin (HG) was 10.1 ± 1.9% (w/w).

A unique emulsification and phase separation process was developed to fabricate nanofibrous heparin-conjugated gelatin microspheres (NHG-MS). After the HG solution was emulsified in mineral oil under rigorous stirring, a precooled isopropanol/1,4-dioxane/ethanol (4/3/1) solvent mixture was added to induce phase separation and subsequently exchange solvents for nanofiber formation. A chemical cross-linking step was further included to stabilize the nanofibrous architecture of the NHG-MS. As shown in Figure 1A–C, the NHG-MS was entirely composed of nanofibers with an average diameter of 223 ± 40 nm, which is on the same scale as natural collagen fibers. Because of the nanofibrous architecture, the NHG-MS had an apparent density of 0.075 $g/cm^3$, which was approximately 8.6% of the SG-MS fabricated using a conventional solvent evaporation method (Figure 1D–G). The lower apparent density of the microsphere generated fewer

Author Manuscript Author Manuscript Author Manuscript Author Manuscript

degradation products when the microsphere degraded. The NHG-MS had a porous structure and exhibited a high porosity of 95.0 ± 0.4%, which was 2.6 times greater than that of the gelatin microsphere with a smooth surface (Figure 1H). A high porosity (often >90%) is desired for the scaffolding material to provide sufficient space for cell growth and ECM deposition. The average size of the NHG-MS was controlled by the stirring speed, and the NHG-MS with a diameter ranging from 90 to 106 $\mu$m, which has excellent injectability and cannot be phagocytosed by macrophages, was selected in all of the experiments described below. The degradation rate of the NHG-MS was controlled by the cross-linking time. Generally, NHG-MS with short cross-linking time had low cross-linking density and high degradation rate (Supporting Information, Figure S2).

### 3.2. IL4 Loading into NHG-MS and Release Profiles.

An immunofluorescence process was developed to visualize the loading and distribution of IL4 in the NHG-MS. To accomplish that, fluorescein isothiocyanate (FITC)-conjugated gelatin was used to prepare the NHG-MS, and IL4 antibody was used to label IL4 protein in the NHG-MS. As shown in Figure 2A–F, IL4 (red) was evenly distributed on the NHG-MS nanofibers (green), indicating the successful loading of the IL4 into the entire NHG-MS.

ELISAs were performed to quantify the loading efficiency and release profile of IL4 from the NHG-MS. For comparison, nanofibrous gelatin microspheres (NG-MS) that were not conjugated with heparin were included in the study. Under the same condition, the NHG-MS had a significantly greater amount of IL4 than the NG-MS (Figure 2G). A typical high burst release profile was detected in the NG-MS group, and more than 62.0 ± 8.7% of the IL4 in the NG-MS was released on the first day (Figure 2H). More than 96.9 ± 1.3% of IL4 was delivered from the NG-MS at day 7, and almost none after 1 week. In contrast, the release profile of IL4 from the NHG-MS was more sustainable, and only 18.2 ± 2.7% of the IL4 was released during the first 24 h. Next, the IL4 in the NHG-MS was constantly released for over 3 weeks, and approximately 75.2 ± 2.3% of the IL4 was released by day 21 (Figure 2H). Obviously, the release profile of the IL4 in the NHG-MS was more controllable than that in the NG-MS.

More importantly, the total detectable amounts of IL4 (including both the released and unreleased IL4) in the NHG-MS and NG-MS were 81.2 ± 6.8 and 38.6 ± 5.0%, respectively (Figure 2I). Because degraded or denatured IL4 cannot be detected by the ELISA, this result indicates that the incorporation of heparin in the microsphere significantly prevented IL4 degradation or denaturation of the NHG-MS.

### 3.3. In Vitro Bioactivity Assay of the IL4 Released from NHG-MS.

The bioactivity of the IL4 released from the NHG-MS was evaluated by bone marrow-derived macrophages (BMDMs). After the BMDMs were polarized into an M1 proinflammatory phenotype stimulated by LPS and IFN-$\gamma$, the BMDMs were exposed to the IL4 released from the NHG-MS at 1 and 14 days. CD68 (a pan-macrophage marker) and CD206 (an M2 macrophage marker) were selected to characterize the BMDM phenotypes. As shown in Figure 3A, the LPS + IFN-$\gamma$ treatment resulted in a rounded M1 phenotype of the BMDMs. After further addition of IL4, the M1 macrophages were changed into

Author Manuscript Author Manuscript Author Manuscript Author Manuscript

$CD206^{+}CD68^{+}$ M2 macrophages characterized by typical elongated spindle shapes. A quantitative analysis indicated that 70% of the proinflammatory M1 macrophages were polarized into anti-inflammatory M2 macrophages ($CD206^{+}CD68^{+}$) after treatment of the IL4 released from the NHG-MS at 1 and 14 days, which was similar to the IL4 positive control (Figure 3B). In contrast, the M2 macrophages were barely detected in the negative control group. ELISA analyses showed that the IL4 released from the NHG-MS resulted in a significant reduction of TNF-$\alpha$ and IL6, two proinflammatory cytokines mainly secreted by the M1 macrophages. Specifically, after the treatment of the IL4 cytokine released from the NHG-MS at 1 and 14 days, the expression of TNF-$\alpha$ reduced to 571.3 ± 62.7 and 606.7 ± 100.5 pg/mL, respectively, which were close to that of the positive control group (539.4 ± 87.9 pg/mL) and significantly lower than that of the LPS + IFN-$\gamma$-only group (1336.3 ± 139.9 pg/mL) (Figure 3C). Similarly, the expressions of IL6 in the IL4 treatment groups were significantly lower than those in the LPS + IFN-$\gamma$-only group (Figure 3D). There was no significant difference between the NHG-MS group and the IL4 positive control group ($P > 0.05$). These results show that the IL4 released from the NHG-MS was able to polarize the M1 macrophage into an M2 phenotype and decrease the production of proinflammatory cytokines (TNF-$\alpha$ and IL6), confirming the high bioactivity of the IL4 released from the NHG-MS.

### 3.4. In Vivo Experiments.

An experimental type 2 diabetes mellitus model was established to simulate the pathogenic process of type 2 diabetes mellitus in humans. A rat mandibular periodontal fenestration model was chosen to evaluate the regulatory effect of the IL4-loaded NHG-MS on macrophage polarization and bone regeneration under a T2DM condition. Under an operating microscope, a mandibular bone defect with a standard size of 3 mm × 2 mm × 1 mm was created and injected with IL4-loaded NHG-MS (Figure 4). CD68 (a pan-macrophage marker), nitric oxide synthase (iNOS, an M1 marker), and CD206 (an M2 marker) double-labeling immunofluorescence staining experiments were performed to identify the phenotype of macrophages within the defective area 7 days after the surgical operation. Overall, the expression of CD68 was significantly higher in the three DM groups than in the normal control group, indicating that more macrophages infiltrated into the defective site of the diabetic rats (Figure 5A–C). However, the expression of iNOS in the IL4-loaded NHG-MS DM group was much lower than that in the other two DM groups, indicating a lower number of M1 macrophages in the IL4-loaded NHG-MS DM group than in the other two DM groups. In addition, the expression of CD206 in the IL4-loaded NHG-MS DM group was similar to that in the normal control group and was much higher than that in the other two DM groups (Figure 5B,E).

Quantitative analyses showed that the total macrophages ($CD68^{+}$) in the DM rat was 1290 ± 177/$mm^2$, compared to 765 ± 116/$mm^2$ in the normal rat (Figure 5C). The total number of macrophages decreased to 1099 ± 105 and 1086 ± 156/$mm^2$ in the NHG-MS and IL4-loaded NHG-MS DM groups, respectively. In addition, the ratio of M1 macrophages ($iNOS^{+}CD68^{+}$) to the total macrophages in the IL4-loaded NHG-MS DM group decreased to 22.7 ± 3.5%, which was significantly lower than that in the DM group (60.4 ± 4.4%) and similar to that in the normal control group (25.6 ± 5.2%) (Figure 5D). Moreover, the ratio of M2

Author Manuscript Author Manuscript Author Manuscript Author Manuscript

macrophages in the IL4-loaded NHG-MS DM group increased to 47.8 ± 4.6%, which was the highest in all four groups (Figure 5E). Consequently, the M2/M1 ratios were 1.68 ± 0.20, 0.36 ± 0.08, 0.28 ± 0.07, and 2.12 ± 0.16 for the normal, DM, DM + NHG-MS, and DM + IL4-loaded NHG-MS groups, respectively (Figure 5F). These results indicated that the incorporation of IL4-loaded NHG-MS in the DM rats significantly promoted the conversion of macrophages from the proinflammatory M1 phenotype to the anti-inflammatory M2 macrophages.

The expression of inflammatory cytokine TNF-$\alpha$, which is mainly secreted by M1 macrophages, was also examined 7 days after the surgical operation. As shown in Figure 6, the expression of TNF-$\alpha$ was strong in the DM and DM + NHG-MS groups, showing the apparent inflammation in these two groups. A significant reduction of TNF-$\alpha$ was observed in the IL4-loaded NHG-MS group. In fact, there was no significant difference in the expression of TNF-$\alpha$ between the IL4-loaded NHG-MS DM and the normal control group. This result confirmed that the IL4-loaded NHG-MS polarized the M1 macrophages into the M2 phenotype and reduced the inflammatory cytokine TNF-$\alpha$ under DM condition.

To further evaluate the effect of the M2/M1 ratio on bone regeneration, immunohistochemical staining was performed for runt-related transcription factor 2 (Runx2), Osterix, and alkaline phosphatase (ALP) 14 days after surgery. The expression of the osteogenic transcription factors Osterix and Runx2 (indicators of cell commitment to an osteogenic lineage) was far more abundant in the normal control group than in the DM group (Figure 7). The implantation of IL4-loaded NHG-MS induced significantly more $Osterix^+$ and $Runx2^+$ osteoprogenitor cells in the defective sites than the NHG-MS group. Although the expression of Osterix and Runx2 was slightly weaker in the IL4-loaded NHG-MS group than in the normal control group, there was no significant difference between them, indicating that the sustained released of IL4 from the NHG-MS effectively enhanced the osteogenic differentiation under DM condition.

Furthermore, as shown in Figure 8, new bone matrix formation just initiated in the DM group 14 days after surgery, whereas the defective sites in the normal control group were filled with new bone matrices. ALP staining, which identifies areas undergoing active mineralization, was broader and stronger in the IL4-loaded NHG-MS group than in the DM and NHG-MS groups. Consistent with the enhanced osteogenic differentiation, the addition of the IL4-loaded NHG-MS improved bone matrix deposition and mineralization under DM condition.

The HE staining and $\mu$-CT results at 4 weeks further confirmed that the bone regeneration was impaired in the presence of diabetes, and the addition of IL4-loaded NHG-MS nearly restored the bone regeneration to normal levels (Figures 9 and 10). The defective site was entirely occupied by new regenerated bone in the normal control group. However, only half of the area of the defect was filled with new bone in the DM group and the rest of the area was occupied by fibrous tissue. The BV/TV ratio of the normal control group was more than twice that of the DM group. The application of IL4-loaded NHG-MS to DM rats increased the BV/TV ratio to 0.44, which was almost 2-fold that in the NHG-MS group (0.23). The slight difference of the ratio BV/TV between the normal control group and the IL4-loaded

Author Manuscript Author Manuscript Author Manuscript Author Manuscript

NHG-MS group might be caused by the remaining microspheres in the defective area. These results demonstrated that the immunomodulatory NHG-MS was an effective biomaterial to modulate the local inflammation, leading to improved bone healing under the DM condition.

## 4. DISCUSSION

Although there are hundreds of millions of diabetic patients who suffer from DM-associated bone fractures and a delayed bone-healing process, research in the scientific community on bone regeneration in DM is limited. Moreover, a number of the efforts on DM-associated bone regeneration have ignored the vital fact that DM is a chronic inflammatory disease and have adopted the similar growth factor-delivery approaches developed for bone regeneration under normal healing conditions. Those approaches are directly targeted at osteoblast or osteoclast cells, and the critical role of inflammation control under diabetic condition was neglected, leading to limited improvement of the healing process.[13,17,36,37] Although several studies examined the delivery of anti-inflammation agents, such as salicylic acid, simvastatin, and tumor necrosis factor (TNF) inhibitors,[38–40] they failed to recognize the fact that impaired macrophage polarization is the fundamental cause of prolonged inflammation, which subsequently suppresses osteogenic differentiation. In this study, we provided a unique immunomodulatory approach that targeted macrophages to accelerate bone healing under DM condition. We designed and synthesized ECM-like injectable gelatin microspheres as an immunomodulatory material that spatiotemporally delivered anti-inflammatory cytokine IL4 to effectively polarize proinflammatory M1 macrophages into an anti-inflammatory M2 phenotype that facilitates osteogenic differentiation and bone formation. Using a DM rat mandibular periodontal fenestration defect model, we showed that this IL4-loading immunomodulatory microsphere system significantly enhanced bone regeneration under diabetic condition.

Inflammatory tissue-resident macrophages are a key regulator of wound healing, and a timely and smooth shift from proinflammatory M1 into anti-inflammatory M2 macrophage is essential for bone regeneration. Under normal healing conditions, a large amount of proinflammatory macrophages infiltrate the defective region in the early stage of fracture healing (0–3 days), resulting in an acute inflammatory response. Subsequently (3–7 days), M1 macrophages gradually change into an anti-inflammatory M2 phenotype, accompanied by resolved inflammation and initiation of tissue regeneration.[41] However, M1 macrophages fail to polarize into an M2 phenotype under diabetic condition. This results in increased production of proinflammatory cytokines, such as TNF-$\alpha$ and IL6, and in return, proinflammatory cells are further recruited to the inflammation site, leading to suppressed osteogenesis. Therefore, regulation of the macrophage to a prohealing M2 phenotype is an appealing approach to reverse delayed DM bone healing. Because IL4 is an effective M2-polarizing cytokine, development of a suitable biomaterial for IL4 delivery is critical to the success of immunomodulation for DM-associated tissue regeneration.

In this work, we designed and synthesized an ECM-like injectable gelatin microsphere as a carrier for IL4. Although there are a variety of nanofabrication technologies, preparation of ECM-like nanofibrous microspheres with the diameters ranging from several to a few hundred micrometers from biodegradable materials has long been a challenge.[42] This is

Author Manuscript Author Manuscript Author Manuscript Author Manuscript

especially difficult for gelatin, which is a water-soluble biomaterial and usually forms microspheres with smooth surfaces (Figure 1D–F). We have recently developed a critical polymer–solvent interaction parameter mathematical model to predict the conditions of nanofiber formation.[43] Guided by this model, we found the approximate solvent compositions (isopropanol/1,4-dioxane/ethanol = 4/3/1) to induce gelatin solution phase separation and successfully fabricated nanofibrous gelatin microspheres (Figure 1A–C). This NHG-MS not only possessed ECM-like architecture but also had a remarkably high surface area and porosity, which is desired for cell adhesion and infiltration. To protect the bioactivity as well as control the release of IL4, we modified gelatin with heparin, which has a binding domain with IL4. A facile coupling reaction between heparin and gelatin was performed, and the decrease of the free amino groups in the gelatin chains demonstrated the success of coupling gelatin with heparin (Figure S1).

The benefits of coupling heparin into NHG-MS were threefold: (a) it provided high loading efficiency of IL4 in microspheres (Figure 2G); (b) it reduced burst release and provided a better release profile for the IL4 in the microsphere (Figure 2H); and (c) it also provided strong protection of IL4 from degradation/denaturation during the release period (Figure 2I). Heparin has high affinity with IL4, which leads to a significant increase in the loading efficiency of IL4 in the NHG-MS. When IL4 was only physically absorbed onto the surface of NG-MS, a high burst release of IL4 was detected in the first 24 h and almost all of the IL4 was released within the first 3 days. In contrast, the NHG-MS showed a more sustainable IL4 release profile over 3 weeks. Approximately 24.8% of the IL4 still remained in the NHG-MS after 3 weeks, suggesting that the NHG-MS, like natural ECM, also served as a reservoir for IL4. Surprisingly, up to 61.4% of the loaded IL4 was not detected in the NG-MS, compared to only 18.1% of the IL4 undetected in the NHG-MS. Because degraded or denatured IL4 cannot be detected by ELISAs, this result indicated that a 3-fold higher amount of IL4 in the NG-MS was degraded or denatured compared to the NHG-MS during the delivery process, highlighting the significant protective role of heparin in NHG-MS.

Although heparin can sequester a number of proteins, including inflammatory cytokines released by immune cells in the tissue regeneration area, IL4 has binding domains with heparin and the preloaded IL4 with the heparin in NHG-MS excludes the potential interactions of heparin with the inflammatory cytokines. In addition, in our scaffolding design, the amount of heparin in the NHG-MS was precisely controlled so that it left no spaces for heparin to sequester inflammatory cytokines at the early stage of the tissue regeneration. Coincidentally, the release of inflammatory cytokines from leukocytes during tissue regeneration mainly occurs in the initial stage (1–3 days) of tissue regeneration. Therefore, the sequestration of inflammatory cytokines in the heparin is minimal in our NHG-MS.

IL4 is a strong regulator of M2 polarization.[44] The in vitro bioactivity assay showed that the M1 macrophages were repolarized to the M2 phenotype upon stimulation of the IL4 released from the NHG-MS (Figure 3). More importantly, the IL4 released from NHG-MS on day 14 had almost the same result as the positive control, indicating that the NHG-MS was capable of retaining high IL4 bioactivity in the microsphere for a long period of time.

Author Manuscript Author Manuscript Author Manuscript Author Manuscript

To further examine the effectiveness of our immunomodulatory IL4-loaded NHG-MS on bone regeneration, a DM-associated rat mandibular periodontal fenestration defect model was created in our study. The inflammatory cytokine TNF-$\alpha$ was used to assess the inflammation during the healing process. One week after the surgery, the expression of TNF-$\alpha$ in the IL4-loaded NHG-MS was similar to that in the normal control group, confirming that the IL4-loaded NHG-MS polarized M1 macrophages to the M2 phenotype and significantly reduced the inflammation under the DM condition. Evaluation of the osteogenic markers (ALP, Osterix, Runx2) confirmed that the IL4-loaded NHG-MS significantly enhanced osteogenesis under the DM condition. The $\mu$-CT analysis and H&E staining further demonstrated that the IL4-loaded NHG-MS restored the bone regeneration close to normal levels. It should be noted that due to the stabilized and protective effects of heparin in the NHG-MS, a low concentration of IL4 (<180 ng/mg NHG-MS) was applied in our in vivo study, which avoided the potential side effects that are often associated with the addition of high-dosage cytokines. All of the results indicated that the IL4-loaded NHG-MS is a promising immunomodulatory biomaterial to accelerate bone healing under DM condition. Although IL4 was used in this study, other cytokines or drugs can be incorporated into NHG-MS with a similar process. The NHG-MS is an excellent injectable carrier for the delivery of various cytokine bioactive molecules and diverse tissue regeneration.

## 5. CONCLUSIONS

We designed and synthesized bioinspired ECM-like NHG-MS as an injectable immunomodulatory biomaterial. The incorporation of heparin in NHG-MS provided binding domains for IL4, protected IL4 bioactivity, and precisely controlled the release of IL4 from the microsphere. The IL4-loaded NHG-MS switched the proinflammatory M1 macrophage into a prohealing M2 phenotype, recovered the M2/M1 ratio to a normal level, efficiently resolved the inflammation, enhanced osteoblastic differentiation, and subsequently restored bone regeneration. The development of immunomodulatory biomaterials, therefore, is a promising approach for bone healing under DM condition.

## Supplementary Material

Refer to Web version on PubMed Central for supplementary material.

## ACKNOWLEDGMENTS

The authors thank Jeanne Santa Cruz for her assistance in editing this article.

Funding

This study was supported by NIH/NIDCR R01DE024979 (X.L.) and China Scholarship Council No. 201606240067 (Z.H.).

## REFERENCES

(1). Guariguata L; Whiting DR; Hambleton I; Beagley J; Linnenkamp U; Shaw JE Global Estimates of Diabetes Prevalence for 2013 and Projections for 2035. Diabetes Res. Clin. Pract 2014, 103, 137–149. [PubMed: 24630390]

Author Manuscript Author Manuscript Author Manuscript Author Manuscript

(2). Chen L; Magliano DJ; Zimmet PZ The Worldwide Epidemiology of Type 2 Diabetes Mellitus-Present and Future Perspectives. Nat. Rev. Endocrinol 2011, 8, 228–236. [PubMed: 22064493]

(3). Szkudelski T; Szkudelska K Resveratrol and Diabetes: From Animal to Human Studies. Biochim. Biophys. Acta 2015, 1852, 1145–1154. [PubMed: 25445538]

(4). Schwartz AV Diabetes Mellitus: Does it Affect Bone? Calcif. Tissue Int 2003, 73, 515–519. [PubMed: 14517715]

(5). Hofbauer LC; Brueck CC; Singh SK; Dobnig H Osteoporosis in Patients with Diabetes Mellitus. J. Bone Miner. Res 2007, 22, 1317–1328. [PubMed: 17501667]

(6). Silva MJ; Brodt MD; Lynch MA; McKenzie JA; Tanouye KM; Nyman JS; Wang X Type 1 Diabetes in Young Rats Leads to Progressive Trabecular Bone Loss, Cessation of Cortical Bone Growth, and Diminished Whole Bone Strength and Fatigue Life. J. Bone Miner. Res 2009, 24, 1618–1627. [PubMed: 19338453]

(7). Janghorbani M; Van Dam RM; Willett WC; Hu FB Systematic Review of Type 1 and Type 2 Diabetes Mellitus and Risk of Fracture. Am. J. Epidemiol 2007, 166, 495–505. [PubMed: 17575306]

(8). Hamann C; Goettsch C; Mettelsiefen J; Henkenjohann V; Rauner M; Hempel U; Bernhardt R; Fratzl-Zelman N; Roschger P; Rammelt S; Gunther KP; Hofbauer LC Delayed Bone Regeneration and Low Bone Mass in a Rat Model of Insulin-Resistant Type 2 Diabetes Mellitus Is due to Impaired Osteoblast Function. Am. J. Physiol.: Endocrinol. Metab 2011, 301, E1220–E1228. [PubMed: 21900121]

(9). von Wilmowsky C; Schlegel KA; Baran C; Nkenke E; Neukam FW; Moest T Peri-implant Defect Regeneration in the Diabetic Pig: A Preclinical Study. J. Cranio-Maxillofac. Surg 2016, 44, 827–834.

(10). Rubin MR; Patsch JM Assessment of Bone Turnover and Bone Quality in Type 2 Diabetic Bone Disease: Current Concepts and Future Directions. Bone Res. 2016, 4, 16001. [PubMed: 27019762]

(11). Loder RT The Influence of Diabetes Mellitus on the Healing of Closed Fractures. Clin. Orthop. Relat. Res 1988, 232, 210–216.

(12). Moy PK; Medina D; Shetty V; Aghaloo TL Dental Implant Failure Rates and Associated Risk Factors. Int. J. Oral Maxillofac. Implants 2005, 20, 569–577. [PubMed: 16161741]

(13). de Santana RB; Trackman PC Effect of Targeted Delivery of Bone Morphogenetic Protein-2 on Bone Formation in Type 1 Diabetes. Int. J. Oral Maxillofac. Implants 2015, 30, 707–714. [PubMed: 26009923]

(14). Jardini MA; Tera TM; Meyer AA; Moretto CM; Prado RF; Santamaria MP Guided Bone Regeneration With or Without a Collagen Membrane in Rats with Induced Diabetes Mellitus: Histomorphometric and Immunolocalization Analysis of Angiogenesis and Bone Turnover Markers. Int. J. Oral Maxillofac. Implants 2016, 31, 918–927. [PubMed: 27447161]

(15). Wallner C; Schira J; Wagner JM; Schulte M; Fischer S; Hirsch T; Richter W; Abraham S; Kneser U; Lehnhardt M; Behr B Application of VEGFA and FGF-9 Enhances Angiogenesis, Osteogenesis and Bone Remodeling in Type 2 Diabetic Long Bone Regeneration. PLoS One 2015, 10, No. e0118823. [PubMed: 25742620]

(16). Picke AK; Salbach-Hirsch J; Hintze V; Rother S; Rauner M; Kascholke C; Moller S; Bernhardt R; Rammelt S; Pisabarro MT; Ruiz-Gomez G; Schnabelrauch M; Schulz-Siegmund M; Hacker MC; Scharnweber D; Hofbauer C; Hofbauer LC Sulfated Hyaluronan Improves Bone Regeneration of Diabetic Rats by Binding Sclerostin and Enhancing Osteoblast Function. Biomaterials 2016, 96, 11–23. [PubMed: 27131598]

(17). Ardura JA; Portal-Nunez S; Lozano D; Gutierrez-Rojas I; Sanchez-Salcedo S; Lopez-Herradon A; Mulero F; Villanueva-Penacarrillo ML; Vallet-Regi M; Esbrit P Local Delivery of Parathyroid Hormone-related Protein-derived Peptides Coated onto a Hydroxyapatite-Based Implant Enhances Bone Regeneration in Old and Diabetic Rats. J. Biomed. Mater. Res., Part A 2016, 104, 2060–2070.

(18). James AW; LaChaud G; Shen J; Asatrian G; Nguyen V; Zhang X; Ting K; Soo C A Review of the Clinical Side Effects of Bone Morphogenetic Protein-2. Tissue Eng., Part B 2016, 22, 284–297.

Author Manuscript Author Manuscript Author Manuscript Author Manuscript

(19). Wynn TA; Barron L Macrophages: Master Regulators of Inflammation and Fibrosis. Semin. Liver Dis 2010, 30, 245–257. [PubMed: 20665377]

(20). Olefsky JM; Glass CK Macrophages, Inflammation, and Insulin Resistance. Annu. Rev. Physiol 2010, 72, 219–246. [PubMed: 20148674]

(21). Dong L; Wang C Harnessing the Power of Macrophages/Monocytes for Enhanced Bone Tissue Engineering. Trends Biotechnol. 2013, 31, 342–346. [PubMed: 23623371]

(22). Spranger J; Kroke A; Mohlig M; Hoffmann K; Bergmann MM; Ristow M; Boeing H; Pfeiffer AF Inflammatory Cytokines and the Risk to Develop Type 2 Diabetes: Results of the Prospective Population-Based European Prospective Investigation into Cancer and Nutrition (EPIC)-Potsdam Study. Diabetes 2003, 52, 812–817. [PubMed: 12606524]

(23). Donath MY; Shoelson SE Type 2 Diabetes as an Inflammatory Disease. Nat. Rev. Immunol 2011, 11, 98–107. [PubMed: 21233852]

(24). Liu X; Ma PX Phase Separation, Pore Structure, and Properties of Nanofibrous Gelatin Scaffolds. Biomaterials 2009, 30, 4094–4103. [PubMed: 19481080]

(25). Liu X; Smith LA; Hu J; Ma PX Biomimetic Nanofibrous Gelatin/Apatite Composite Scaffolds for Bone Tissue Engineering. Biomaterials 2009, 30, 2252–2258. [PubMed: 19152974]

(26). Sachar A; Strom TA; Serrano MJ; Benson MD; Opperman LA; Svoboda KK; Liu X Osteoblasts Responses to Three-Dimensional Nanofibrous Gelatin Scaffolds. J. Biomed. Mater. Res., Part A 2012, 100, 3029–3041.

(27). Ma C; Jing Y; Sun H; Liu X Hierarchical Nanofibrous Microspheres with Controlled Growth Factor Delivery for Bone Regeneration. Adv. Healthcare Mater 2015, 4, 2699–2708.

(28). Lortat-Jacob H; Garrone P; Banchereau J; Grimaud JA Human Interleukin 4 Is a Glycosaminoglycan-Binding Protein. Cytokine 1997, 9, 101–105. [PubMed: 9071560]

(29). Li Z; Qu T; Ding C; Ma C; Sun H; Li S; Liu X Injectable Gelatin Derivative Hydrogels with Sustained Vascular Endothelial Growth Factor Release for Induced Angiogenesis. Acta Biomater. 2015, 13, 88–100. [PubMed: 25462840]

(30). Sachar A; Strom TA; San Miguel S; Serrano MJ; Svoboda KK; Liu X Cell-Matrix and Cell-Cell Interactions of Human Gingival Fibroblasts on Three-Dimensional Nanofibrous Gelatin Scaffolds. J. Tissue Eng. Regener. Med 2014, 8, 862–873.

(31). Zhang X; Goncalves R; Mosser DM The Isolation and Characterization of Murine Macrophages. Curr. Protoc. Immunol 2008, 14.1.1.

(32). Reed MJ; Meszaros K; Entes LJ; Claypool MD; Pinkett JG; Gadbois TM; Reaven GM A New Rat Model of type 2 Diabetes: the Fat-Fed, Streptozotocin-Treated Rat. Metabolism 2000, 49, 1390–1394. [PubMed: 11092499]

(33). Padial-Molina M; Rodriguez JC; Volk SL; Rios HF Standardized In Vivo Model for Studying Novel Regenerative Approaches for Multitissue Bone-Ligament Interfaces. Nat. Protoc. 2015, 10, 1038–1049. [PubMed: 26086406]

(34). Wang L; Aghvami M; Brunski J; Helms J Biophysical Regulation of Osteotomy Healing: An Animal Study. Clin. Implant Dent. Relat. Res 2017, 19, 590–599. [PubMed: 28608504]

(35). Li C; Williams BO; Cao X; Wan M LRP6 in Mesenchymal Stem Cells Is Required for Bone Formation during Bone Growth and Bone Remodeling. Bone Res. 2014, 2, 14006. [PubMed: 26273519]

(36). Wang F; Song YL; Li CX; Li DH; Zhang HP; Ma AJ; Xi XQ; Zhang N; Wang BG; Wang Y; Zhou W Sustained Release of Insulin-like Growth Factor-1 from Poly(lactide-co-glycolide) Microspheres Improves Osseointegration of Dental Implants in Type 2 Diabetic Rats. Eur. J. Pharmacol 2010, 640, 226–232. [PubMed: 20438725]

(37). Al-Zube L; Breitbart EA; O'Connor JP; Parsons JR; Bradica G; Hart CE; Lin SS Recombinant Human Platelet-Derived Growth Factor BB (rhPDGF-BB) and Beta-Tricalcium Phosphate/ Collagen Matrix Enhance Fracture Healing in a Diabetic Rat Model. J. Orthop. Res 2009, 27, 1074–1081. [PubMed: 19170096]

(38). Yu W; Bien-Aime S; Mattos M; Alsadun S; Wada K; Rogado S; Fiorellini J; Graves D; Uhrich K Sustained, Localized Salicylic Acid Delivery Enhances Diabetic Bone Regeneration via Prolonged Mitigation of Inflammation. J. Biomed. Mater. Res., Part A 2016, 104, 2595–2603.

Author Manuscript Author Manuscript Author Manuscript Author Manuscript

(39). Ezirganli Ş; Kazancioglu HO; Mihmanli A; Aydin MS; Sharifov R; Alkan A The Effect of Local Simvastatin Application on Critical Size Defects in the Diabetic Rats. Clin. Oral Implants Res 2014, 25, 969–976. [PubMed: 23600677]

(40). Wang Q; Li H; Xiao Y; Li S; Li B; Zhao X; Ye L; Guo B; Chen X; Ding Y; Bao C Locally Controlled Delivery of TNF-alpha Antibody from a Novel Glucose-Sensitive Scaffold Enhances Alveolar Bone Healing in Diabetic Conditions. J. Controlled Release 2015, 206, 232–242.

(41). Schlundt C; El Khassawna T; Serra A; Dienelt A; Wendler S; Schell H; van Rooijen N; Radbruch A; Lucius R; Hartmann S; Duda GN; Schmidt-Bleek K Macrophages in Bone Fracture Healing: Their Essential Role in Endochondral Ossification. Bone 2018, 106, 78–89. [PubMed: 26529389]

(42). Liu X; Jin X; Ma PX Nanofibrous Hollow Microspheres Self-Assembled from Star-Shaped Polymers as Injectable Cell Carriers for Knee Repair. Nat. Mater 2011, 10, 398–406. [PubMed: 21499313]

(43). Ma C; Liu X Formation of Nanofibrous Matrices, Three-Dimensional Scaffolds, and Microspheres: From Theory to Practice. Tissue Eng., Part C 2017, 23, 50–59.

(44). Mia S; Warnecke A; Zhang XM; Malmstrom V; Harris RA An Optimized Protocol for Human M2 Macrophages Using M-CSF and IL-4/IL-10/TGF-beta Yields a Dominant Immunosuppressive Phenotype. Scand. J. Immunol 2014, 79, 305–314. [PubMed: 24521472]

Author Manuscript Author Manuscript Author Manuscript Author Manuscript

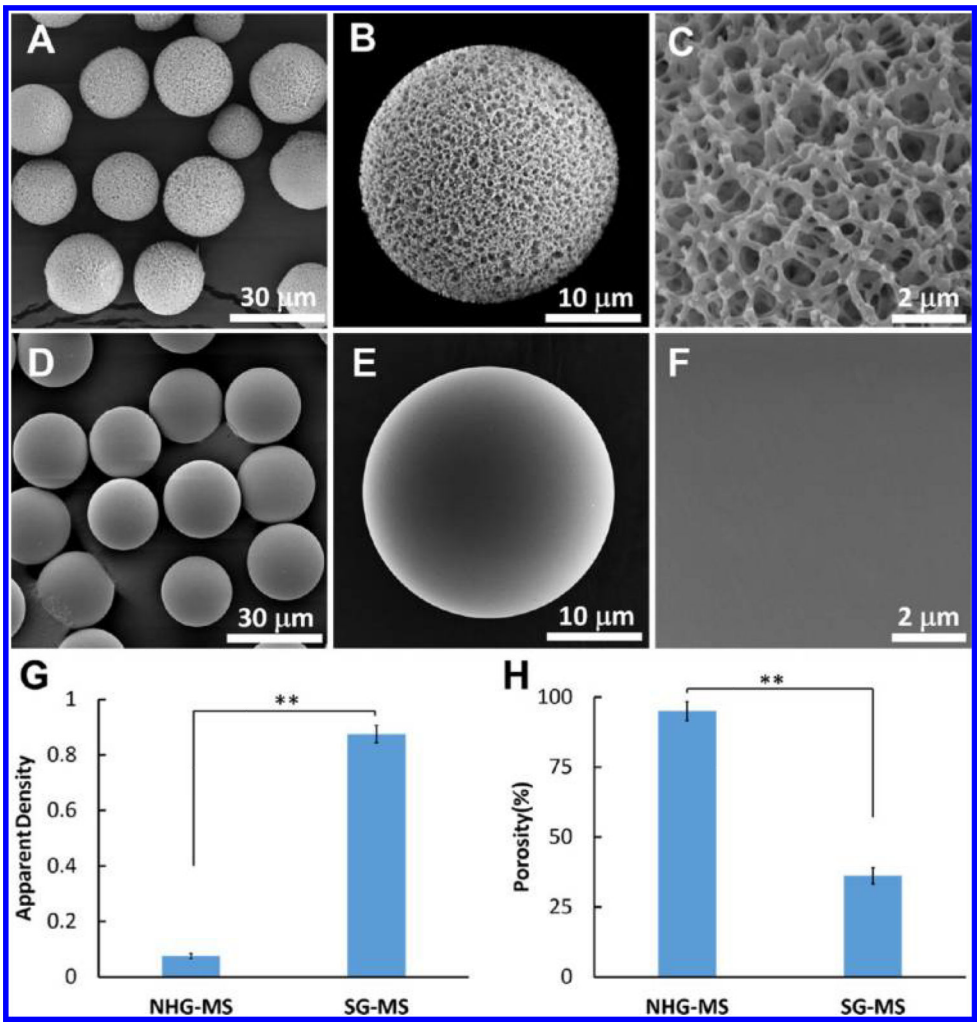


**Figure 1.**

Characterizations of NHG-MS and SG-MS. (A–C) SEM images of NHG-MS, showing the highly porous nanofibrous architecture. (D–F) SEM images of solid gelatin microspheres (SG-MS), showing the smooth surface architecture. (G–H) Apparent density and porosity of NHG-MS and SG-MS (** $P < 0.01$).

Author Manuscript Author Manuscript Author Manuscript Author Manuscript

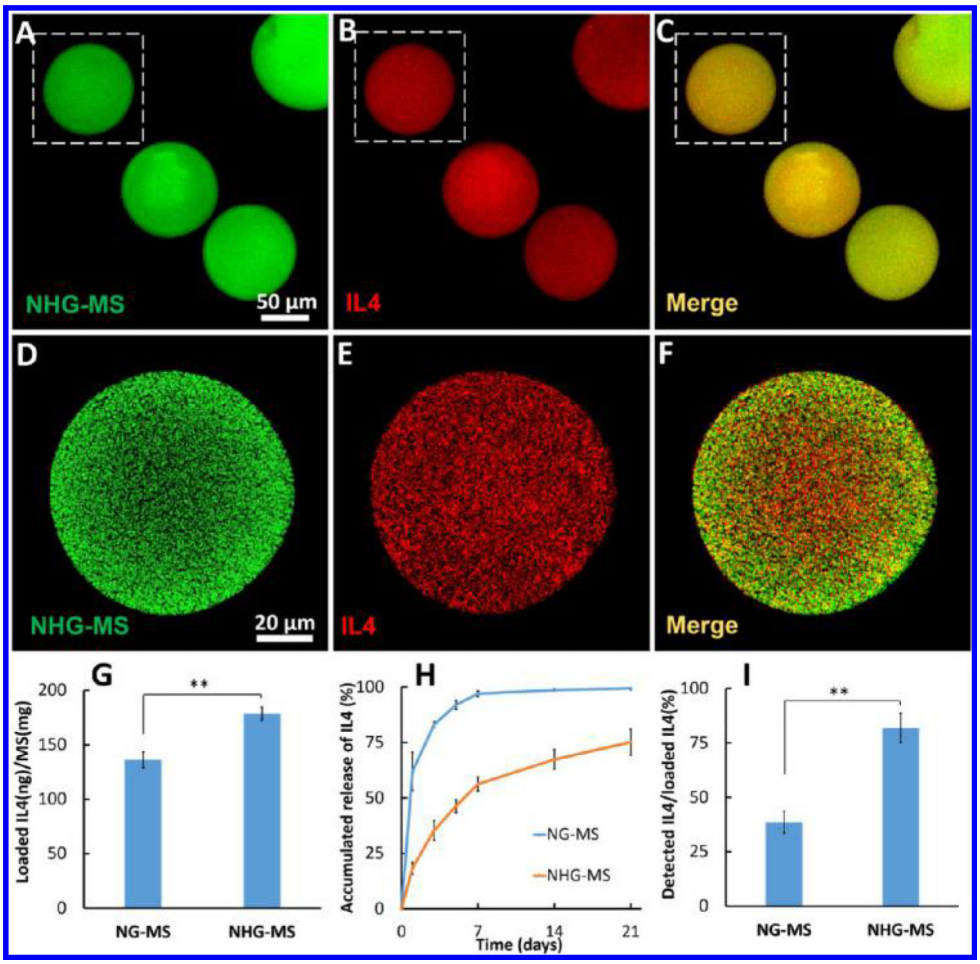


**Figure 2.**

Characterizations of IL4-loaded NHG-MS and NG-MS and their release profiles. (A–C) Stacked confocal images of IL4-loaded NHG-MS. (D–F) Cross-sectional confocal images at a higher magnification, showing that IL4 (red) was evenly distributed in the NHG-MS (green). (G) Loading efficiency of IL4 in NHG-MS and NG-MS. (H) Release profiles of IL4 from NHG-MS and NG-MS. (I) Total amount of IL4 (released and unreleased) from the NHG-MS and NG-MS detected via an ELISA (** $P < 0.01$).

Author Manuscript Author Manuscript Author Manuscript Author Manuscript

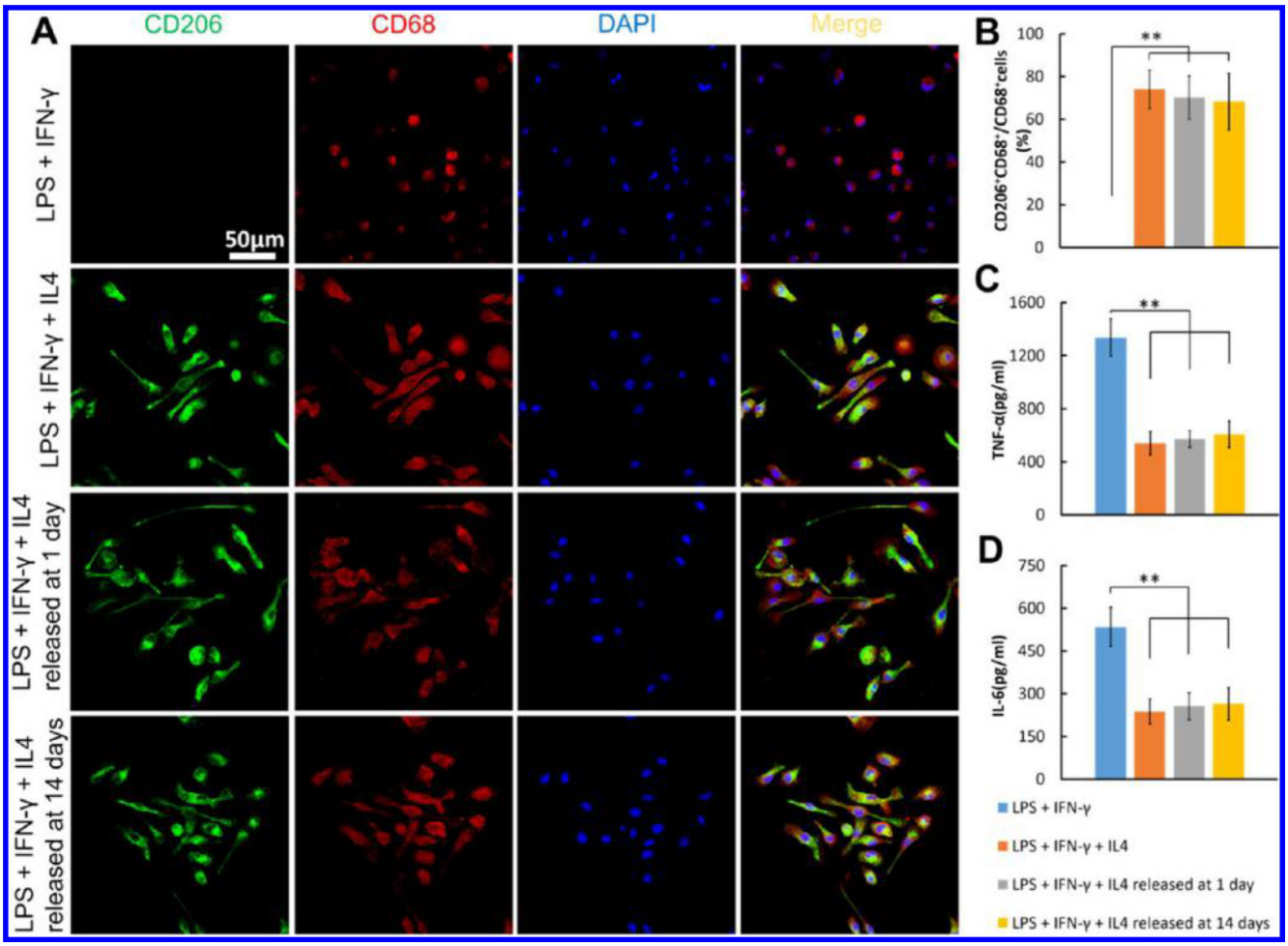


**Figure 3.**

In vitro bioactivity assay of the IL4 released from NHG-MS. Bone marrow-derived macrophages (BMDMs) stimulated by LPS and IFN-$\gamma$ for 24 h were polarized into M1 proinflammatory macrophages and then exposed to IL4 released from NHG-MS at 1 and 14 days for 24 h. The LPS + IFN-$\gamma$-only and the LPS + IFN-$\gamma$ + IL4 groups were used as negative and positive controls, respectively. (A, B) Immunofluorescence images and quantitative analysis of $CD206^+$ (green, an M2 macrophage marker) and $CD68^+$ (red, pan-macrophage marker) BMDMs. Cells treated with the LPS + IFN-$\gamma$-only group exhibited a rounded morphology, and $CD206^+$ cells were barely detected in this negative control group, indicating the proinflammatory M1 phenotype. By contrast, addition of IL4 released from NHG-MS at 1 and 14 days switched the cells into typical elongated spindle shapes, and approximately 70% BMDMs were $CD206^+CD68^+$ M2 phenotype, which was similar to the IL4 positive control group. (C, D) Quantitative analysis of proinflammatory cytokines in the supernatant showed the significant reduction of both TNF-$\alpha$ and IL6 in three groups with additional IL4 treatment (**$P < 0.01$).

Author Manuscript Author Manuscript Author Manuscript Author Manuscript

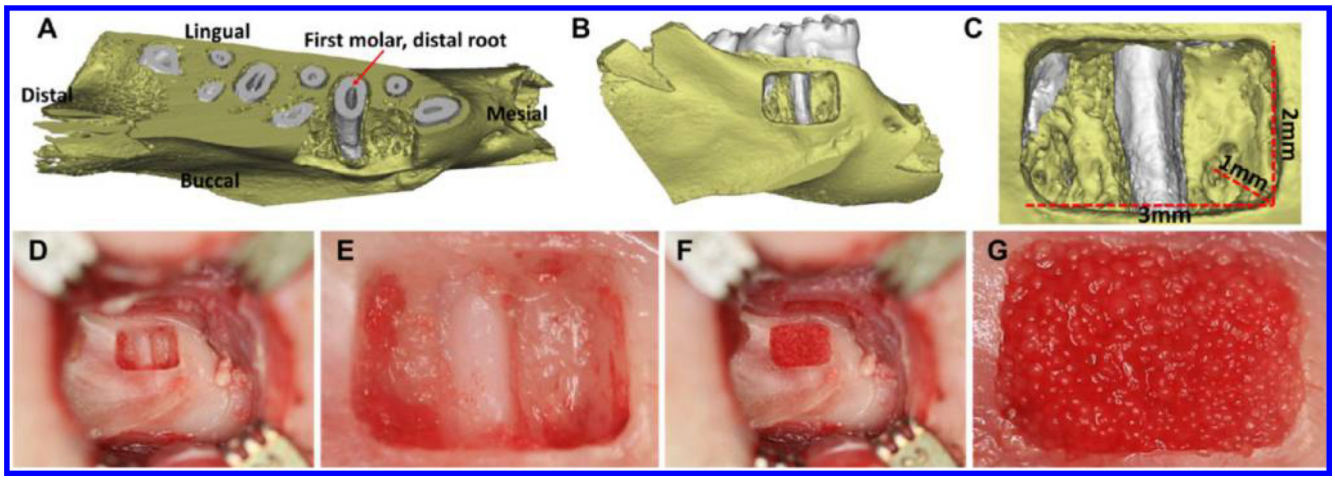


**Figure 4.**

Generation and characterization of rat mandibular periodontal fenestration model. (A–C) $\mu$-CT three-dimensional reconstruction images of the mandibular defect model shows that the defect with standard size of 3 mm × 2 mm × 1 mm was located on the buccal side of the first and second molars of the rat. The distal root (white) of the rat mandibular first molar was exposed in the middle of the defect. (D–G) Photographs of a rat mandible after creation of the defect (D, E) and the implantation of NHG-MS in the defect region (F, G).

Author Manuscript Author Manuscript Author Manuscript Author Manuscript

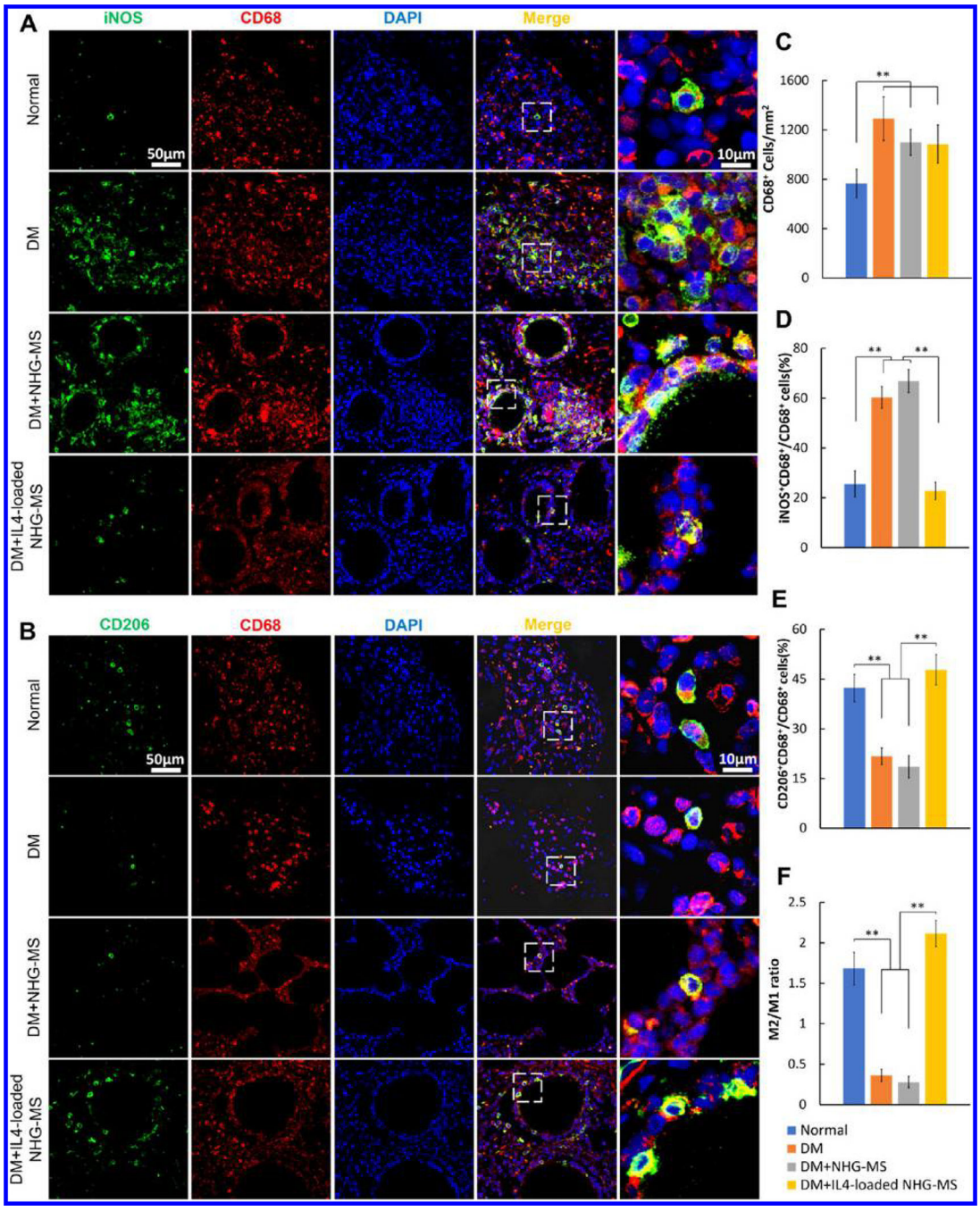


**Figure 5.**

Macrophage phenotype in the defect area 7 days after surgical operation: iNOS (green, an M1 macrophage marker); CD206 (green, an M2 macrophage marker); and CD68 (red, pan-macrophage marker). (A) Immunofluorescence images showed that iNOS was extensively expressed in the DM and DM + NHG-MS groups. In comparison, the expression of iNOS in the IL4-loaded NHG-MS DM group was much less, which is similar to the normal control group, indicating fewer M1 macrophages in the normal control and IL4-loaded NHG-MS DM groups than the other two DM groups. (B) Immunofluorescence images showed that the

Author Manuscript Author Manuscript Author Manuscript Author Manuscript

expression of CD206 in the IL4-loaded NHG-MS DM group was similar to that in the normal control group and much higher than that in the other two DM groups. (C–F) Quantitative analysis showed that the expression of CD68 was significantly higher in the three DM groups than that in the normal control group (C), indicating that more macrophages infiltrated into the defect site of diabetic rats. Fewer M1 macrophages and more M2 macrophages in both the normal control and IL4-loaded NHG-MS DM groups (D, E) resulted in significantly higher M2/M1 ratios than in the other two DM groups (F) (** $P <$ 0.01).

Author Manuscript Author Manuscript Author Manuscript Author Manuscript

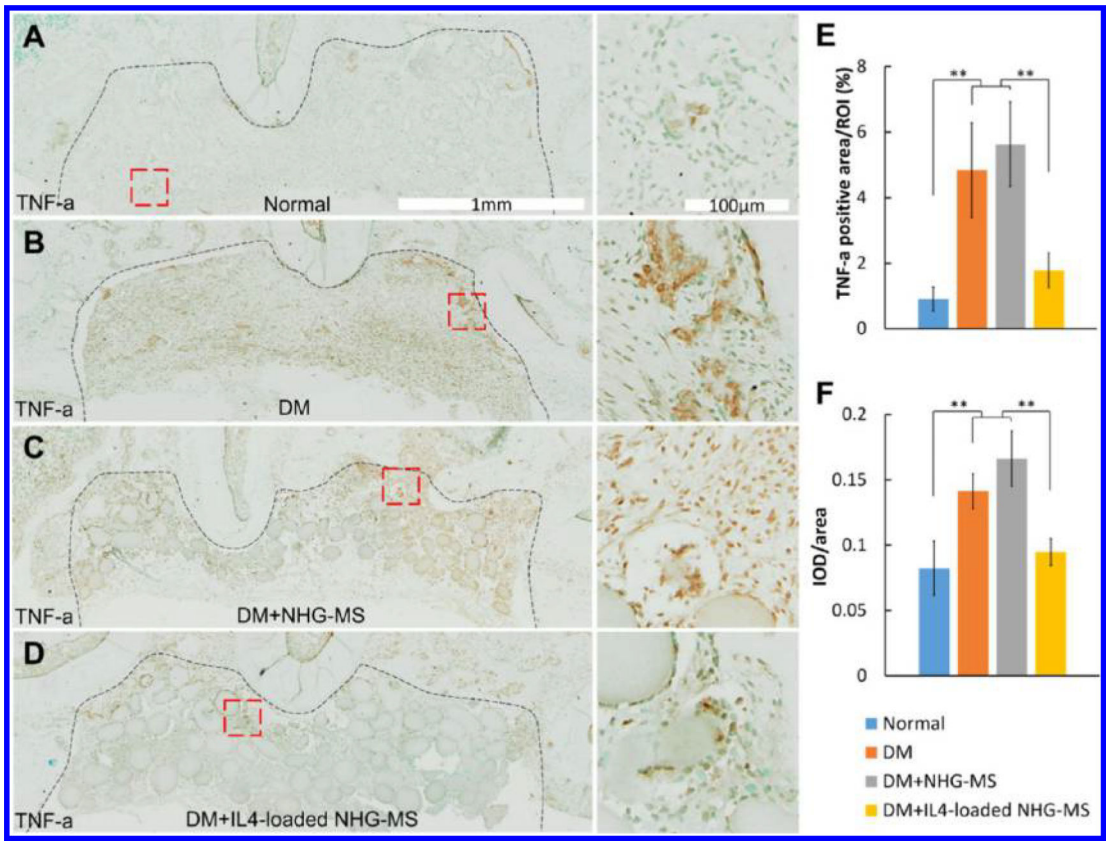


**Figure 6.**

Expression of proinflammatory cytokines TNF-$\alpha$ in the defect area 7 days after the surgical operation. (A–D) Immunohistochemical images showed stronger expression of TNF-$\alpha$ in DM and DM + NHG-MS groups than in normal control and IL4-loaded NHG-MS DM groups. (E, F) Quantitative analysis of TNF-$\alpha$ positive area ratio and mean integral optical density (IOD) (**$P < 0.01$).

Author Manuscript Author Manuscript Author Manuscript Author Manuscript

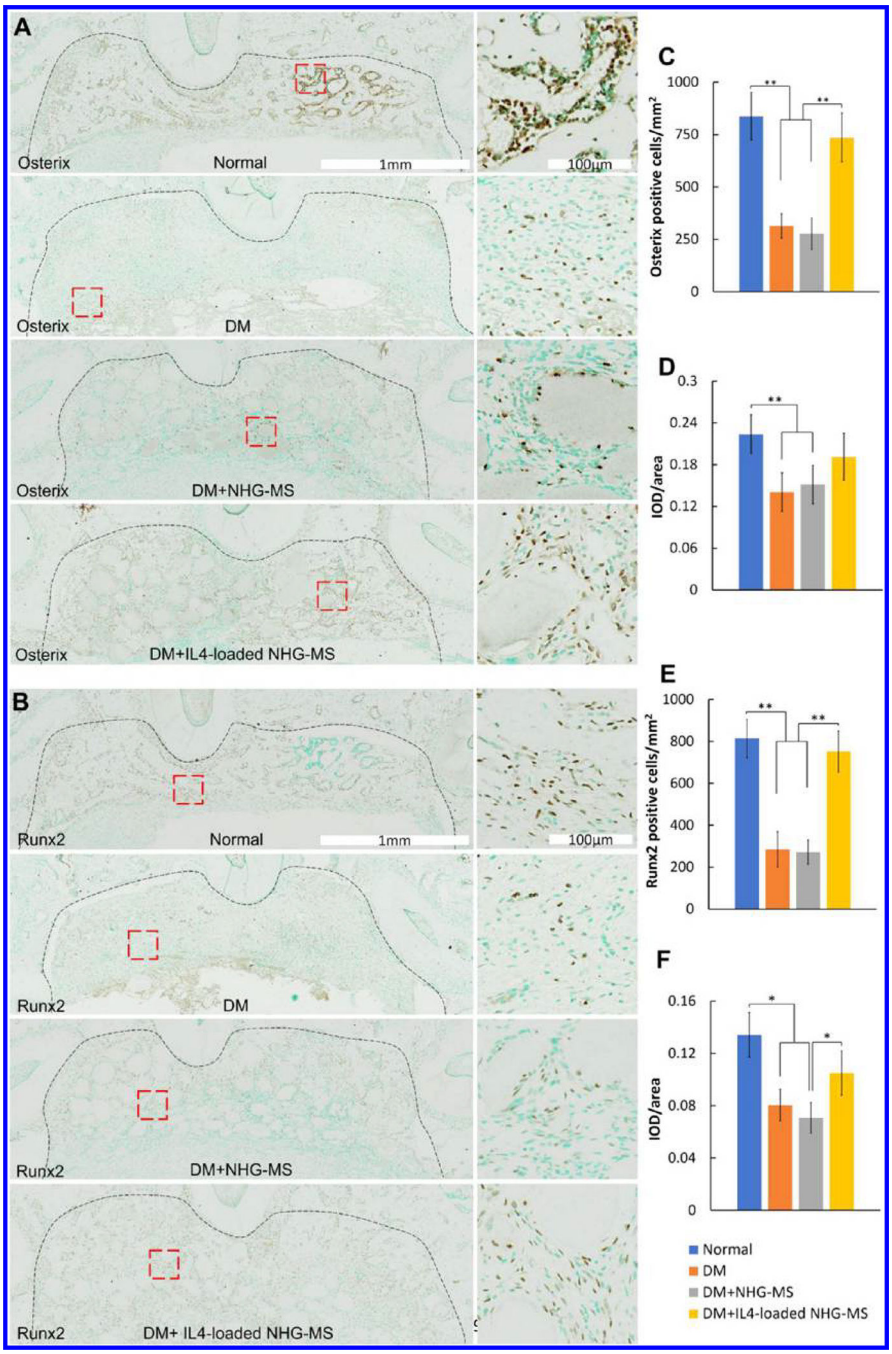


**Figure 7.**

Expression of Osterix and Runx2 in the defect area 14 days after the surgical operation. (A, B) Immunohistochemical images showed significantly more Osterix$^+$ and Runx2$^+$ osteoprogenitor cells in normal control and IL4-loaded NHG-MS DM groups than in the other two DM groups. (C–F) Quantitative analysis of the number of Osterix$^+$ and Runx2$^+$ cells and mean integral optical density (IOD) (*$P < 0.05$, **$P < 0.01$).

Author Manuscript Author Manuscript Author Manuscript Author Manuscript

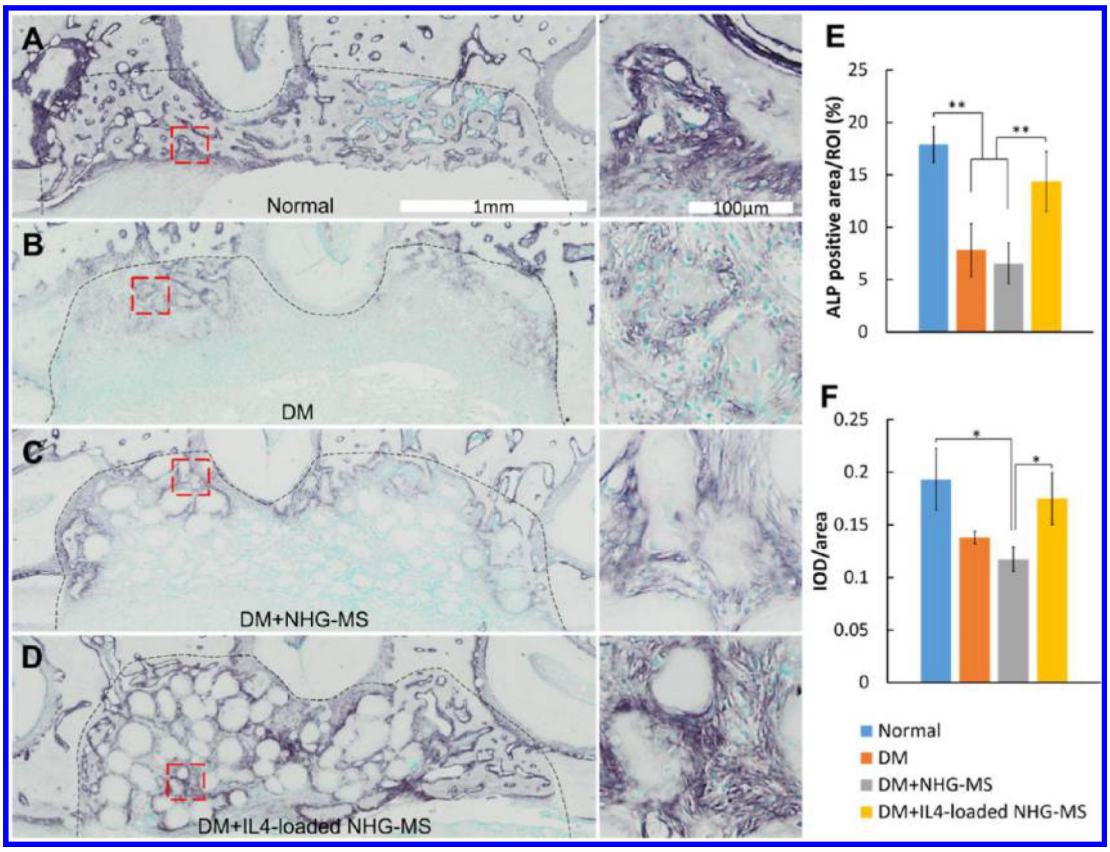


**Figure 8.**

ALP staining of the defect area 14 days after the surgical operation. (A–D) Normal control and IL4-loaded NHG-MS DM groups exhibited significantly more extensive and robust ALP expression than in the other two DM groups. (E, F) Quantitative analysis of ALP-positive area ratio and mean integral optical density (IOD) (*$P < 0.05$, **$P < 0.01$).

Author Manuscript Author Manuscript Author Manuscript Author Manuscript

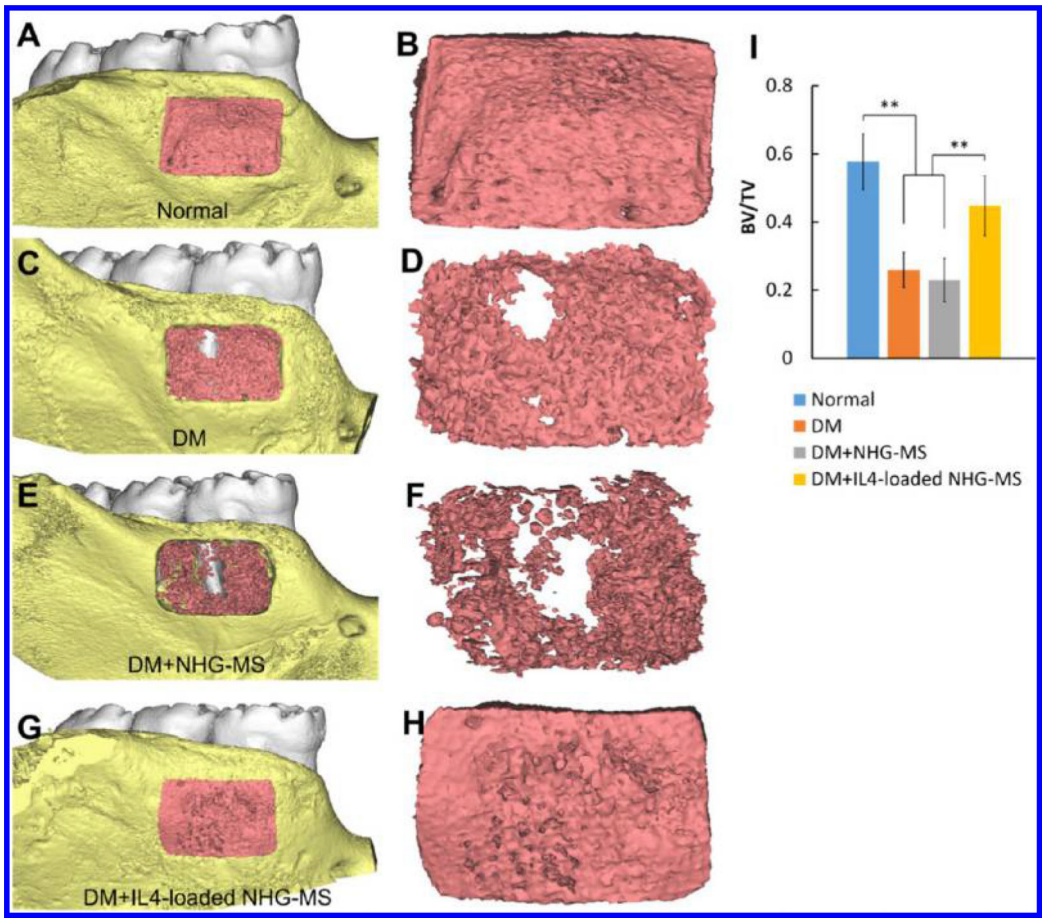


**Figure 9.**

$\mu$-CT three-dimensional reconstruction images of the rat mandible and new regenerated bone 4 weeks after surgery. (A–H) The defect area was entirely occupied by new regenerated bone in both the normal control group and the IL4-loaded NHG-MS DM group. In contrast, only half of the defect region was filled with new bone in the DM and DM + NHG-MS groups. (I) Ratio of bone volume to total volume (BV/TV) in all four groups (** $P < 0.01$).

Author Manuscript Author Manuscript Author Manuscript Author Manuscript

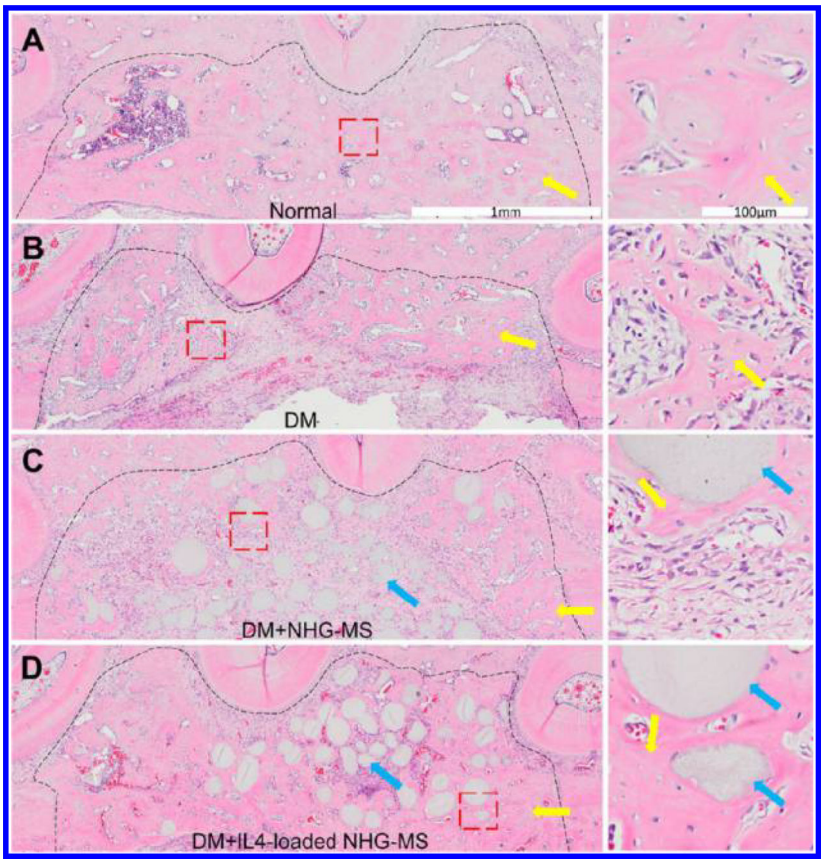


**Figure 10.**

HE staining of the defect area 4 weeks after the surgical operation. (A–D) Newly formed bone filled the entire defect area in the normal control and the IL4-loaded NHG-MS DM group. In comparison, new bone formation was observed on the outer boundary of the defect area in the DM and DM + NHG-MS groups. The yellow arrows indicate newly formed bone, and the blue arrows indicate microspheres.

Author Manuscript Author Manuscript Author Manuscript Author Manuscript

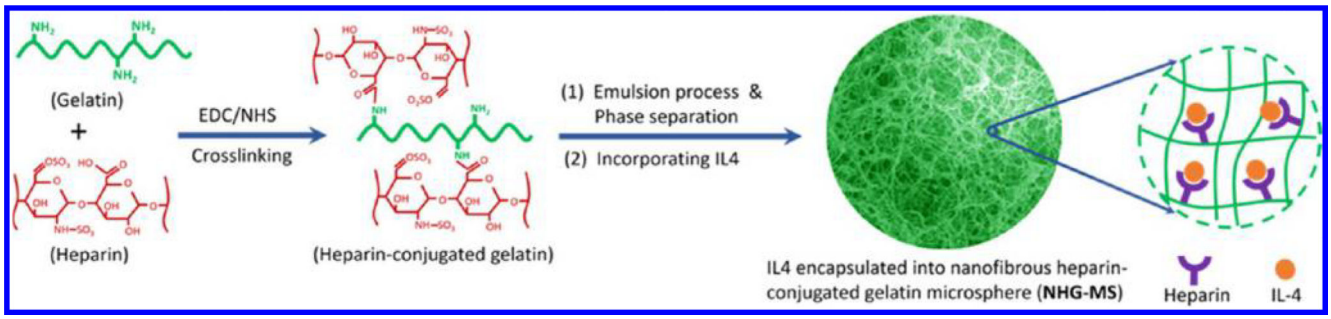


**Scheme 1.**

Schematic Illustration of Preparation of IL4-Loaded NHG-MS[a]

[a]NHG-MS is fabricated via a combined emulsion and phase separation process, and IL4 is incorporated in the NHG-MS via binding with heparin in the microsphere.